

Power uprates
and plant life extension

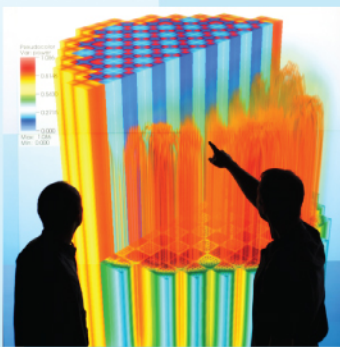


CASL-W2014-0040-000



Consortium for Advanced Simulation of LWRs

Engineering design
and analysis



L3:THM.CLS.P7.07

Transient Evolution of Bubbles in a Channel

Science-enabling
high performance
computing



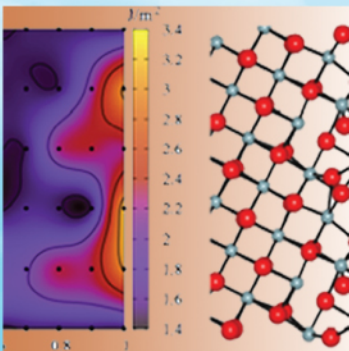
Jiacai Lu and

Gretar Tryggvason

University of Notre Dame

November 30, 2013

Fundamental science



Plant operational data



U.S. DEPARTMENT OF
ENERGY

Nuclear Energy

Transient Evolution of Bubbles in a Channel

L3:THM.CLS.P7.07 milestone report

*Jiacai Lu¹
Gretar Tryggvason²*

¹*Worcester Polytechnic Institute*
²*University of Notre Dame*

November 30, 2013 (Ver. 1.1)

Abstract: Transient motion of bubbles is studied using direct numerical simulations. Three aspects of bubbly flows in vertical channels are examined: The lateral motion of nearly spherical bubbles rising in shear flow toward a wall and the motion of deformable bubbles away from the wall; the effect void fraction of the lateral motion of nearly spherical and deformable bubbles toward or away from a wall; and the initial transient motion of a large number of bubbles in turbulent channel flow. The first sets of results compliment an earlier study of the steady state drag and lift of buoyant bubbles in vertical shear and show that the motion of nearly spherical bubbles remains essentially unaffected by the wall for bubbles whose centroid is more than a bubble diameter away from the wall. The presence of other bubbles affects the migration of nearly spherical bubbles toward a wall and the motion of deformable bubbles from the wall but further studies are needed to fully elucidate the effect. The results for the large channel flow show an evolution toward the steady state void fraction distribution examined earlier, but that the modification of the void fraction seems to take place considerably faster than the change in the velocity profile.

Contents

<i>LIST OF FIGURES</i>	4
<i>LIST OF TABLES</i>	5
1. <i>RELEVANCE TO CASL AND OBJECTIVES</i>	6
3. <i>COMPUTATIONAL SETUP</i>	6
4. <i>RESULTS</i>	7
5. <i>FUTURE WORK</i>	19
<i>APPENDIX: DESCRIPTION OF THE NUMERICAL CODE</i>	21

List of Figures

Figure 1. Computational domain and control forces.

Figure 2. The flow field around bubbles held fixed in a shear flow.

Figure 3. The lift coefficient versus the distance to the wall, using the moving domain method.

Figure 4. Spherical cap bubble rising in initially quiescent flow. The bubble results from starting with an oblate spheroid and allowing it to evolve freely.

Figure 5. The horizontal location and the velocity of the center of the bubbles in figure 1 versus time. The results are presented in computational units.

Figure 6. The lateral drift velocity versus shear rate for the two cases in Table I, where the bubbles remain nearly spherical.

Figure 7. Simulations of several bubbles near a wall. The focus is on estimating the effect of the other bubbles on the bubble in the middle.

Figure 8. The horizontal location (top) and the bubble horizontal velocity (bottom) for the simulations shown in figure 7. The red line indicates the bubble in the middle.

Figure 9. Bubbles in the large run at times 4, 16 and 34.

Figure 10. Trajectories of y-coordinates of selected bubbles. The frame on the left shows the four biggest bubbles (Left: 4 bubbles with $d=0.4414$; Middle: 13 bubbles with $d=0.3856$; Right: 50 bubbles with $d=0.306$).

Figure 11. The bubbles and the vorticity at times 4, 16 and 34.

Figure 12. The mean streamwise liquid velocity across the channel at different times.

Figure 13. The Reynolds stresses (normalized by $(u^+)^2$, where u^+ is the friction velocity) across the channel at different time steps.

Figure 14. The void fraction at three different times, along with the predictions of a simple model for the void fraction at steady state.

Figure 15. The streamwise vorticity squared (normalized by $1/t_0^2$, where t_0 is a reference time equal to μ/τ_w) across the channel at different time steps.

Figure 16. The streamwise velocity fluctuations (normalized by u^+ , where u^+ is the friction velocity) across the channel at different time steps.

Figure 17. The wall-normal velocity fluctuations (normalized by u^+ , where u^+ is the friction velocity) across the channel at different time step.

Figure 18. Turbulent Kinetic Energy (normalized by $(u^+)^2$) across the channel.

Figure 19. Dissipation Rate (normalized by $(u^+)^4/\nu$) across the channel.

List of Tables

Table I. The lateral drift velocity for two sets of simulations where the shear velocity is changed.

Table II. The distribution of bubble sizes for the large run described in this section. The bubble diameter is in computational units.

1. Relevance to CASL and Objectives

Development and validation of closure laws for computational multiphase fluid dynamics (CMFD) is a necessary part of successful prediction of reactor thermal hydraulics behavior. The presented study demonstrates the capabilities of the advanced numerical tools to determine the essential closure parameters in a range of conditions. Further studies can enhance the parametric space and fill in the gaps in the available experimental database.

2. Computational Setup

The computations are done using the FTC3D code briefly described in the appendix. The computational domain is a rectangular channel where the inflow at the top is specified, the left and right boundaries are rigid no-slip walls with a given velocity and periodic boundary conditions are used in the spanwise direction. The computational domain, shown in Figure 2, is the same as used for our earlier simulations except that in many cases the force in the vertical direction is kept constant and the computational domain is moved as the bubbles rises, to keep it roughly in the center.

To gravitational forces used to keep the bubble stationary are adjusted by a PID (proportional-integral-derivative) controller based on the location and velocity of the bubble centroid. At every time step, the new values are found by:

$$g_x^{\alpha+1} = g_x^\alpha - c_{Px}(x - x_0) - c_{Ix} \int (x - x_0) dt - c_{Dx} U_b$$

$$g_y^{\alpha+1} = g_y^\alpha - c_{Py}(y - y_0) - c_{Iy} \int (y - y_0) dt - c_{Dy} V_b$$

For most of the calculations reported in our last report we used the following control parameters:

$$c_{Px} = 0.02; c_{Ix} = 0.01; c_{Dx} = 0.02$$

$$c_{Py} = 0.03; c_{Iy} = 0.02; c_{Dy} = 0.05$$

In many of the simulations reported here, the vertical gravity is fixed and the domain is moved with the bubble. Once gravity acceleration has been determined, the lift and drag coefficients can be determined by balancing the buoyancy and lift or drag. The lift force is given by:

$$F_L = -C_L \rho \frac{\pi d^3}{6} (V_b - V_L) \times \Omega_L \text{ where } |\Omega_L| = \frac{\Delta V}{L}$$

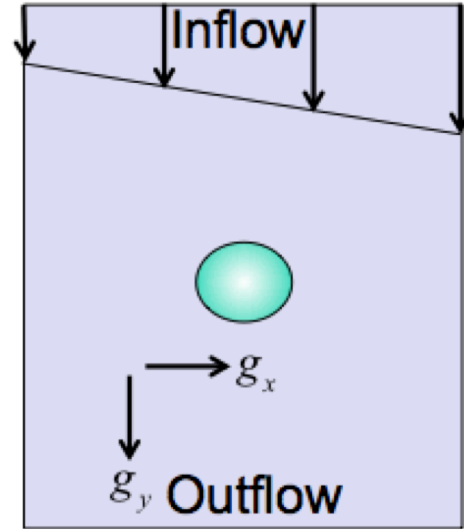


Figure 1. Computational domain and control forces.

The buoyancy force in the horizontal direction is:

$$F_B = \Delta\rho \frac{\pi d^3}{6} g_x$$

$$F_L = -C_L \rho \frac{\pi d^3}{6} (V_b - V_L) \times \Omega_L \text{ where } |\Omega_L| = \frac{\Delta V}{L}$$

and at steady state the buoyancy balances the lift, $F_B = F_L$. We can isolate the lift coefficient, resulting in:

$$C_L = \frac{\Delta\rho g_x L}{\rho V_L \Delta V} \text{ where } |\Omega_L| = \frac{\Delta V}{L}$$

Similarly, the drag in the vertical direction is:

$$F_D = C_D \frac{\pi d^2}{8} \rho V_b^2$$

which must be balanced by buoyancy in the vertical direction. Thus

$$C_D = \frac{4 d \Delta\rho g_y}{3 \rho V_b^2}$$

The various non-dimensional numbers are defined as:

$$Re = \frac{\rho d V_b}{\mu}; \quad Eo = \frac{\Delta\rho g d^2}{\sigma}; \quad M = \frac{\Delta\rho g \mu^4}{\rho^2 \sigma^3}; \quad G = \frac{\rho d^2 \Delta V}{\mu L};$$

3. Results

In our last report we described result from computations of the forces on a single bubble. The bubble was placed in a channel bounded by vertical walls and a prescribed inflow. The outflow boundary conditions were selected to minimally disrupt the upstream flow. To hold the bubble steady we adjusted gravitational forces in both the horizontal and vertical direction using a PID controller as described above. Once a steady state had been reached, the lift and drag is balanced by buoyancy so the forces are easily found. One shortcoming of this approach, particularly for examining the changes of the forces as a bubble is moved closer to a wall, is that the vertical gravitational force must be changed. This results in a change in the governing nondimensional numbers and thus the results for different distances to the wall will apply to different bubbles. To alleviate this problem we have changed the setup slightly and instead of holding the bubble stationary in the vertical direction we now allow it to rise freely, but

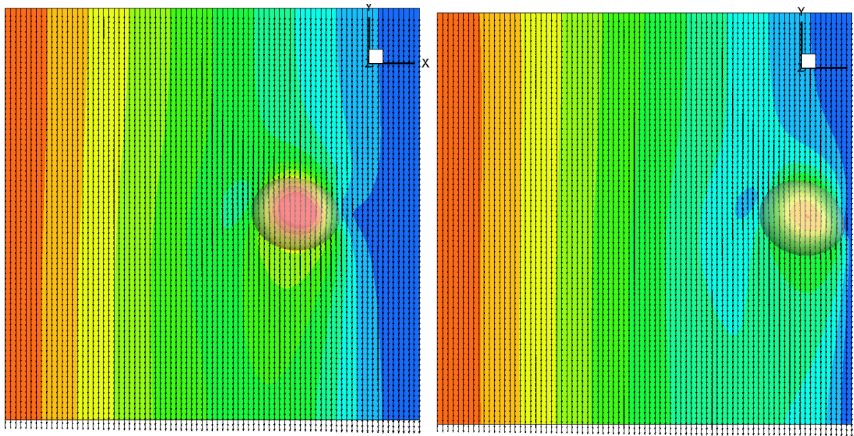


Figure 2. The flow field around bubbles held fixed in a shear flow.

move the computational domain with it, keeping the relative bubble location approximately constant. Thus, if the bubble slows down when it is moved to the wall, the speed of the domain is reduced, but the gravitational force in the vertical direction and the nondimensional numbers that involve the

gravitational acceleration stay the same. We have confirmed that this new setup results in the same lift and drag coefficients as the earlier setup. To find the steady state lift and drag we still adjust the horizontal gravity coefficient to keep the horizontal location fixed. Figure 2 shows two examples of the flow field around a single bubble at steady obtained using the moving domain method, and figure 3 shows how the lift coefficient depends on the nondimensional distance of the bubble center from the wall. As found earlier, it rapidly changes from positive to negative very close to the wall.

We have also expanded the range of nondimensional parameters and, for example, simulated a few large bubbles that take on a spherical cap shape as they rise. The difficulty with simulating bubbles in this parameter range is that often the final shape depends on the initial conditions. An initially spherical bubble can, for example, result in a toroidal bubble

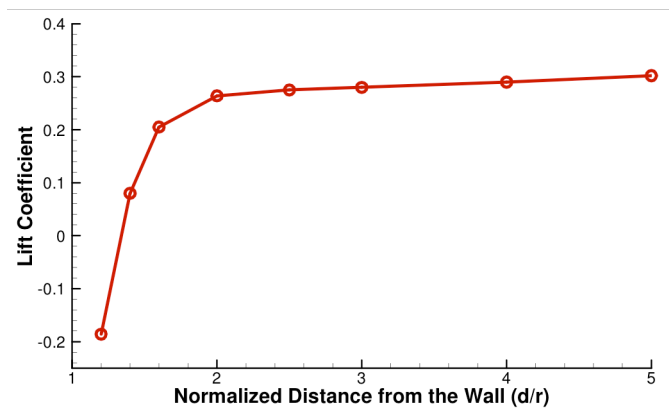


Figure 3. The lift coefficient versus the distance to the wall, using the moving domain method.

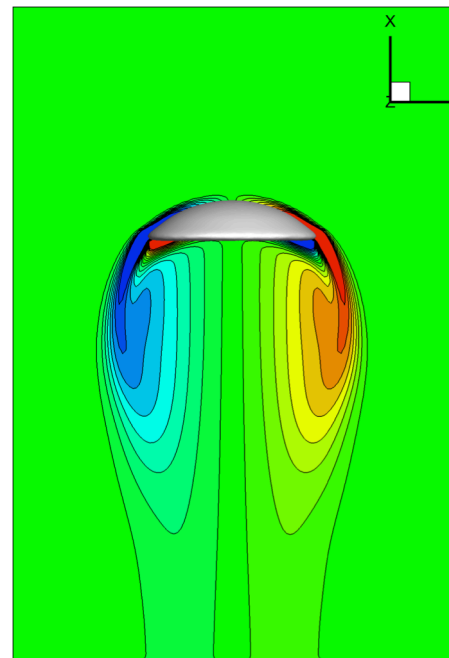


Figure 4. Spherical cap bubble rising in initially quiescent flow. The bubble results from starting with an oblate spheroid and allowing it to evolve freely.

rather than a spherical cap. To get a spherical cap bubble it is necessary to start with a different shape, such as an oblate bubble. Figure 2 shows one example of a spherical cap bubble rising in a quiescent flow (no shear). In addition to the bubble, the vorticity in a plane cutting through the center of the bubble is shown. Here the Morton number is 4.83×10^{-5} , the Eotvos number is 80, and the density and viscosity ratios are 100 and 50 respectively, resulting in a rise Reynolds number of 192. This compares well with theoretical estimates, which give a rise Reynolds number of about 200. So far we have not examined the effect of shear on bubbles in this parameter range, but we anticipate that they will remain intact for only relatively small shear rates.

The motion of bubbles in shear toward/away from a wall

The motion of bubbles near walls is of critical importance in many applications involving bubbly flows. In some cases bubbles are generated near wall as in boiling and in other cases strong shear near walls modifies the bubble distribution due to shear-induced lift. For bubbly upflows in vertical channels, for example, it is well known that while small bubbles accumulate near walls, more deformable bubbles move away from the walls.

In our earlier studies we examined the forces (lift and drag) on stationary bubbles in shear flow and how the forces change as the bubbles are moved closer to the walls. The rate at which spherical bubbles move toward walls and deformable bubbles move away from walls is obviously also of significant importance. One of most significant questions is when the presence of the wall starts to impact the motion of the bubble and here we focus on examining nearly spherical bubbles moving toward a wall. The computational setup is the same as in our studies of lift and drag except that we only specify fixed gravity acceleration and move the computational domain with the bubble, which also is free to move in the horizontal direction. The simulations have been run using “computational units,” usually selected to be relatively close to unity. The dimensionless form of the results allows a comparison with physical variables.

We have examined several cases. The deformability of the bubbles was changed by changing the surface tension, the shear rate was changed by modifying the inlet and the vertical wall velocities. Since nearly spherical bubbles move toward the wall and deformable bubbles generally move away from the wall, the nearly spherical bubbles were initially located near the center of the channel and the deformable ones were located at the wall. Since the shear rate influences how the bubbles deform and whether they move toward or away from the wall, in some cases we tested both initial conditions and picked the one appropriate for the subsequent motion of the bubble.

Figure 5 shows the horizontal location and the velocity of three bubbles moving toward the wall. The horizontal location is shown on the left (the wall is at $y=1$) and the horizontal drift velocity across the channel is shown on the right. The shear rate increases from the top to the bottom. The bubbles are initially placed near the middle of the channel and after an initial transient where the flow adjusts to the presence of the bubble it is clear that it approaches the wall with the nearly constant velocity. Indeed,

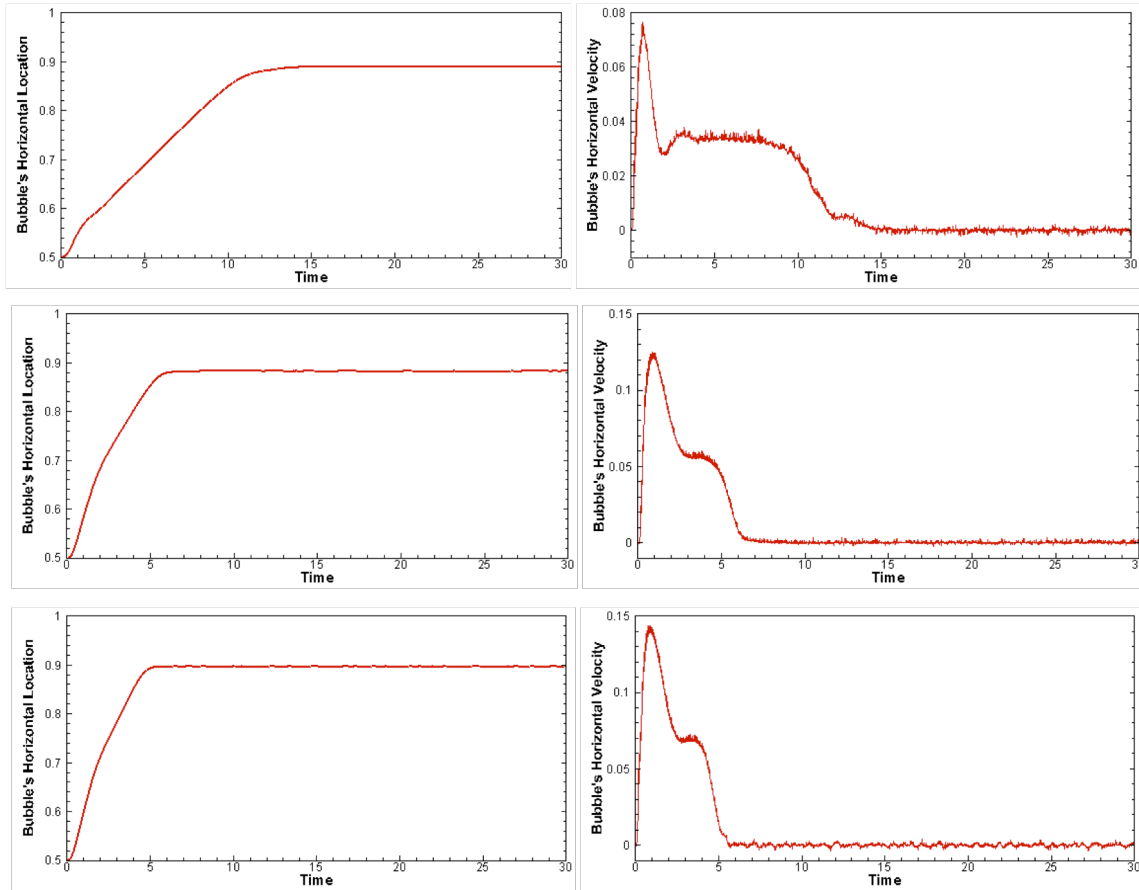


Figure 5. The horizontal location and the velocity of the center of the bubbles in figure 1 versus time. The results are presented in computational units.

the center of the bubble is less than a bubble diameter away from the wall when the bubble approaching the wall shows any signs of slowing down and similarly, the bubble moving away from the wall reaches a nearly steady horizontal velocity at about the same location. The length of the transient region increases with the shear rate and in the bottom frame the region of constant velocity is relatively short. We have also experimented with first holding the bubble fixed by adjusting a gravitational force in the horizontal direction and then putting it equal to zero when the flow has reached a steady state. This reduces the length of the initial transient but does not eliminate it. For strong shear rates we expect to have to release the bubbles far from the walls.

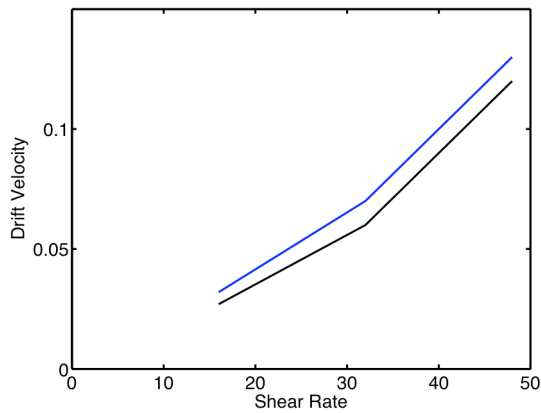


Figure 6. The lateral drift velocity versus shear rate for the two cases in Table I, where the bubbles remain nearly spherical.

Eo	Log M	Gr	Vel
1.56	-5.6	16	0.027
"	"	32	0.06
"	"	48	0.12
0.52	-7.04	16	0.032
"	"	32	0.07
"	"	48	0.13

Table I. The lateral drift velocity for two sets of simulations where the shear velocity is changed.

We have examined the motion of bubbles in shear to and from a wall for several other values of the control parameters, such as Morton number and nondimensional shear rate and figure 6 and Table I shows the approach velocity for three different shear rates and two sets of different Morton and Eotvos numbers. It is clear that increasing shear rate increases the approach velocity, as we expect, but while the velocity initially increases linearly so that it doubles when we double the shear rate, for higher shear rates the approach velocity increases faster. A more detailed examination of even higher shear rates remains to be done. The most important conclusion for the parameters presented here, however, is that the velocity is generally constant until the bubble is almost at the wall for approaching bubbles and that it quickly reaches a constant value for departing bubbles. Thus, it seems that in most cases the bubbles simply approach the walls unaware of its presence until they collide with it, and that departing bubbles move as in unbounded flow as soon as they leave the wall. This obviously simplifies modeling bubble motion near walls considerably.

We have compared the horizontal velocity to predictions for the drift of bubbles using a simple lift force models, using lift coefficients obtained for single bubbles in simple shear flow and generally find reasonable agreement.

For more deformable bubbles the bubble/wall interactions appear to be more complex and while we have done simulations for several such cases, we have not completed the analysis yet.

Simulations of dense bubble systems

To assess the effect of large void fraction, we have done several simulations where we place several bubbles close to each other. Since the bubbles move with different velocities and we move the domain to keep the bubbles in the middle, we focus on one bubble and use the others simply to increase the void fraction around it. Figure 7 shows two frames for one case with nearly spherical bubble that move toward the wall. The bubble in the middle, marked with an "X" is the bubble that we focus on and in figure 8 we plot its distance to the wall versus time. The presence of the other bubbles first increases

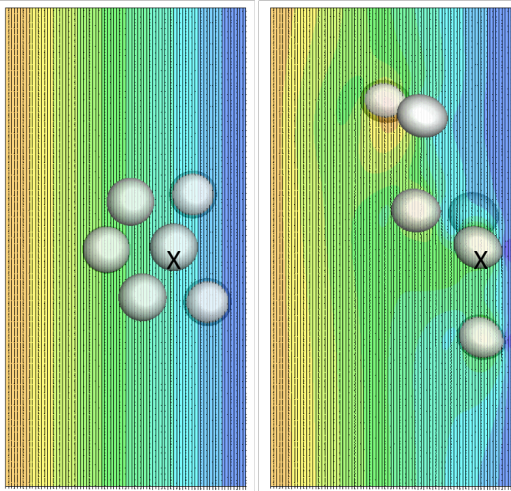


Figure 7. Simulations of several bubbles near a wall. The focus is on estimating the effect of the other bubbles on the bubble in the middle.

the velocity of the reference bubble to the wall as compared with a single bubble. Once a bubble is close enough to the wall so that there are no bubbles between it and the wall, bubbles further away move past it since the velocity increases with the distance to the wall and as they pass they push the reference bubble toward the wall. We have done other simulations where we put the bubbles surrounding the bubble that we focus on in different positions, but keeping the “local void fraction” the same. While the results are similar, generally the initial transient makes it difficult to get consistent results, even though the setups are comparable. We are currently examining other possibilities to determine the effect of the void fraction. Those include using a larger number of bubbles and/or holding the reference bubbles steady initially before releasing it to allow the flow to adjust to its presence. Another possibility is to gather the data by sampling large-scale simulations such as those presented in the next section. Preliminary results for sampling large simulations are described in J. Lu and G. Tryggvason. Dynamics of nearly spherical bubbles in a turbulent channel upflow. *Journal of Fluid Mechanics* 732 (2013), 166-189.

Transient evolution of a large number of bubbles

The systems examined above are relatively simple and intended to allow us to examine one specific interaction between the bubbles and the flow. To study a more realistic system, where multiple bubbles interact with turbulent flow and other bubbles of different sizes, we present here results for a much larger system. These simulations, which are currently being done using 2048 processors on the Titan have, however, only been carried out for a relatively short time so far.

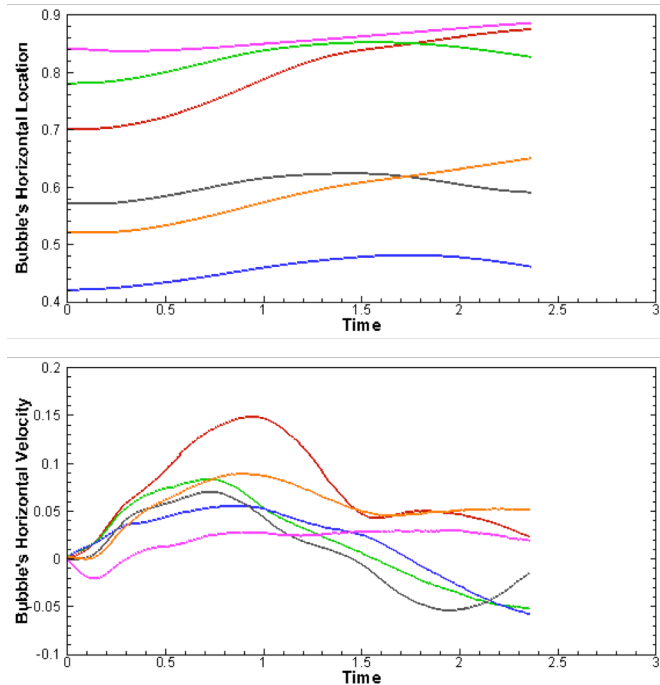


Figure 8. The horizontal location (top) and the bubble horizontal velocity (bottom) for the simulations shown in figure 7. The red line indicates the bubble in the middle.

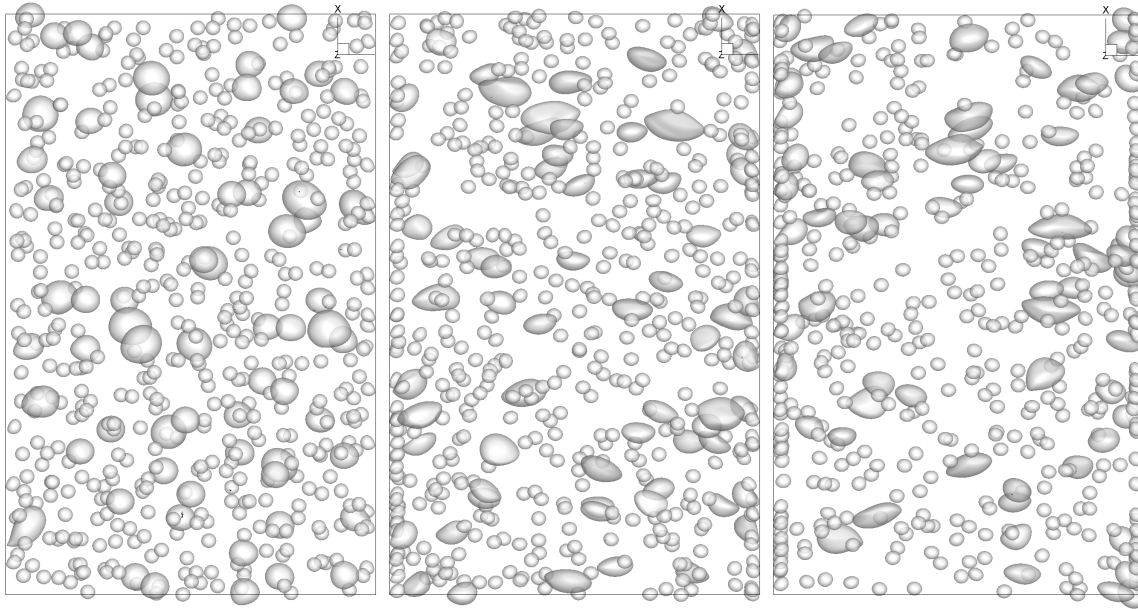


Figure 8. Bubbles in the large run at times 4, 16 and 34.

Figure 8 shows the flow of many bubbles of different size at one relatively early time ($t=13$, in computational units). The domain size is $2\pi \times 4 \times \pi$ in the streamwise, wall normal and spanwise direction, respectively, resolved by $1024 \times 768 \times 512$ grid points. The grid is uniform in the streamwise and spanwise direction, but in the wall-normal direction it is stretched to give a finer resolution near the walls. The physical parameters are selected such that the Morton number is equal to 5.75×10^{-10} . The bubbles come in four sizes, as listed in Table II. The majority of bubbles are small and since our earlier results suggest that the transition between bubbles pushed to the wall and those that are not is around $Eo=2.5$, we would expect the smallest two bubbles to accumulate at the wall. The numbers were selected such that there are enough small bubbles that can be pushed to the wall to put the core in hydrostatic equilibrium. The properties of the fluid and the bubbles are the same as in our earlier simulations, but the domain size is eight times larger, giving a friction Reynolds number of $Re^+ = 500$. The bubbles are initially distributed nearly uniformly across the domain but as they start to rise, the smaller bubbles start to migrate toward the walls and form a dense wall layer. At the second and third time plotted we see that there are already several small bubbles, and a few of the slightly larger ones, that have been pushed to the wall. The largest bubbles, however, stay in the middle of the channel.

Number of Bubbles	Diameter of Bubbles	Eotvos Number
4	0.4414	3.805
13	0.3856	2.904
50	0.306	1.829
504	0.16	0.50

Table II. The distribution of bubble sizes for the large run described in this section. The bubble diameter is in computational units.

The motion of the bubbles is also seen in figure 10, where we plot the horizontal location of the bubbles versus time (vertical axis). The four frames show, from the left, the four largest bubbles, the thirteen

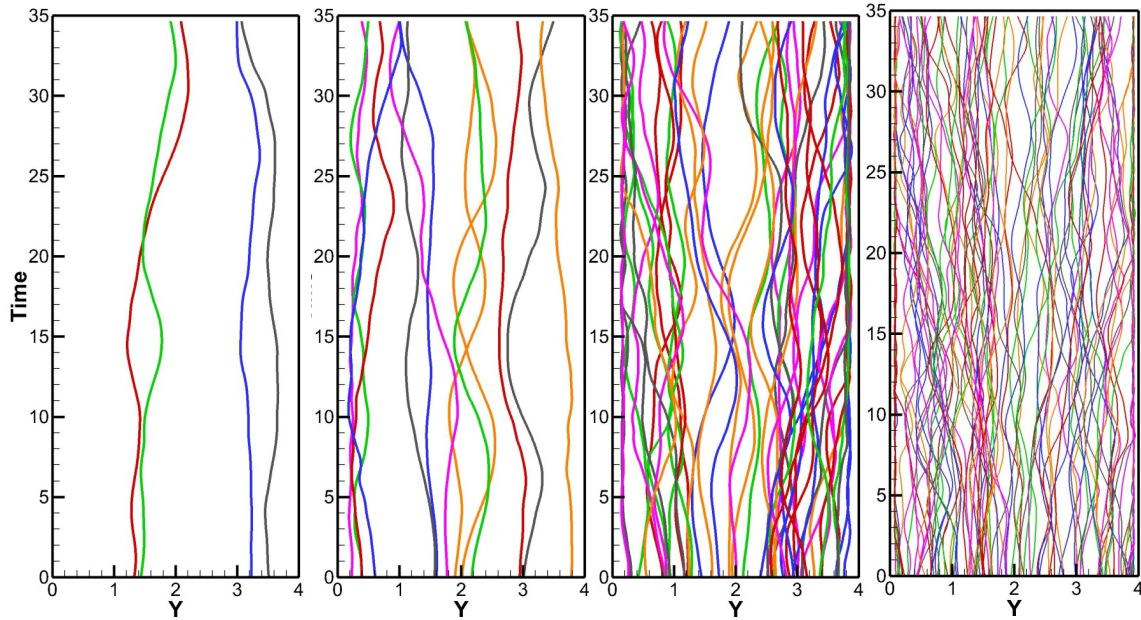


Figure 10. Trajectories of y -coordinates of selected bubbles. The frame on the left shows the four biggest bubbles (Left: 4 bubbles with $d=0.4414$; Middle: 13 bubbles with $d=0.3856$; Right: 50 bubbles with $d=0.306$).

slightly smaller ones, the fifty even smaller bubbles and finally, in the frame on the right, we show the path of some of the smallest ones. There are 504 small bubbles and we have only plotted 100 of them since plotting all in the same frame obscures the view completely. We have also plotted the path of the other small bubbles and believe that the paths shown here are representative. A careful inspection of the plots confirms that the largest bubbles have not been rearranged to any significant degree by the motion but the smallest bubbles generally have moved out of the middle of the channel toward the walls. This is slightly clearer in the plot of the fifty, second smallest bubbles, but the plot for the smallest bubbles shows several bubbles paths converging on the wall.

Figure 11 shows the vorticity (and the bubbles) using the lambda-2 method to visualize the vorticity. It is clear that the vorticity is increased initially as the bubbles start to move. The vertical structures in the first figure correspond roughly to what we would expect in a single phase flow, since that is the initial velocity and it takes some time for the bubbles to modify the flow. Although the bubbles in the second and third frame have added considerable vorticity in the interior of the domain, the wall vorticity has not been modified significantly.

The average streamwise velocity is plotted in figure 12 and it is clear here that the average velocity remains relatively unchanged. This is expected since the small bubbles must first move to the wall to form a layer there before the presence of the layer starts to influence the velocity. As the flow evolves further, however, we expect the presence of the bubbles at the wall to reduce the flow rate. Experience with bubbles in turbulent upflow at smaller Reynolds numbers and in smaller systems suggest that this will take significant time.

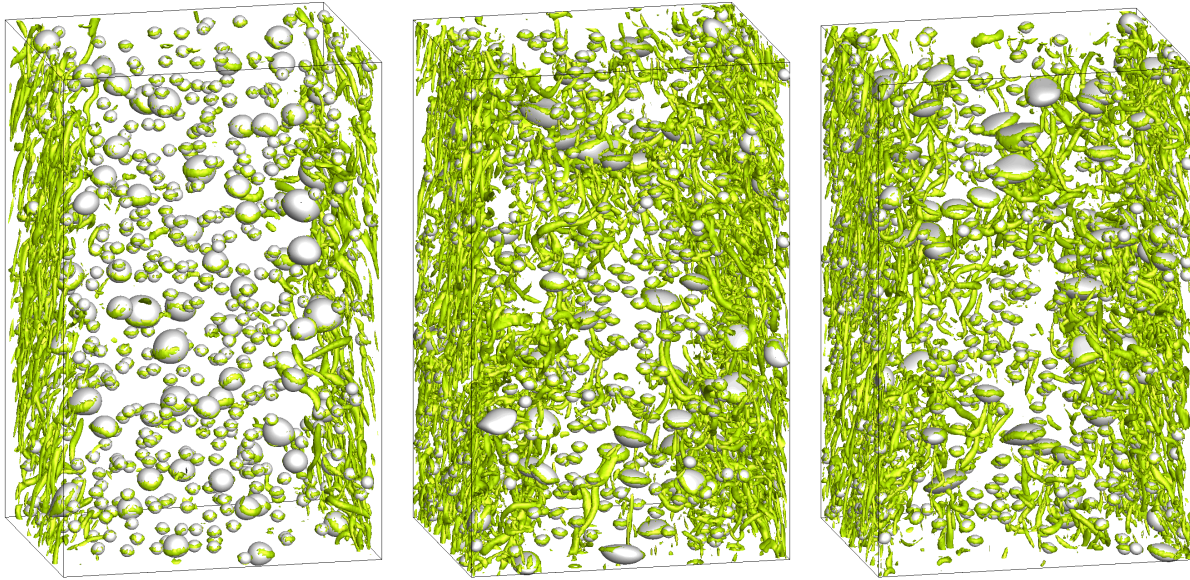


Figure 11. The bubbles and the vorticity at times 4, 16 and 34.

The lack of modification of the flow due to the presence of the bubbles at this time is also seen in figure 13, where the turbulent shear $\langle u'v' \rangle$ is plotted versus the horizontal coordinate. Although the average profile changes slightly, it shows the linear shape expected for a single-phase flow for all three times. If the flow reaches a steady state that is similar to what we have seen for smaller systems and lower Reynolds numbers, we expect that it would eventually become zero, on the average, in the middle of the channel.

The fact that the void fraction changes before the average velocity is supported by figure 14 which shows the void fraction at three different times, along with the predictions of the simple model for the void fraction at steady state originally presented in our earlier work. Initially the bubbles are relatively uniformly distributed but as the bubbles start to move upward the small bubbles start to migrate toward the wall. This leads to an increase in the void fraction there, although at the latest time it is clear that the distribution has not reached the steady state value.

To examine in more details the changes that the bubbles cause in the vorticity distribution in the channel, we plot the average streamwise vorticity squared in figure 15 for the three times examined earlier. Two changes take place between the early time and the two later times. First of all, the vorticity in the center of the channel increases, as the bubbles start to move and generate vorticity. Secondly, the structure of the vorticity near the wall starts to change. At the earliest time we see the vorticity distribution we expect for a single phase flow, that is a peak close to the wall corresponding to hairpin vortices and then a maximum right at the wall corresponding to the wall bound vorticity needed to bring the velocity to zero. When the bubbles move toward the wall this changes and we see a significant increase in the vorticity near the wall. The peak near the wall due to the hairpin vortices is also no longer as clearly visible.

The change in velocity fluctuations is explored the next two figures where we plot the streamwise velocity fluctuations (figure 16) and the wall-normal velocity fluctuations (figure 17) versus the horizontal coordinate. As expected the presence of the bubbles increases the velocity fluctuations in the middle of the channel. The bubbles also increase the wall-normal fluctuations near the wall, but the streamwise fluctuations are mostly unchanged for the times examined here.

For turbulence modeling we need the turbulent kinetic energy, figure 18, and the dissipation rate, figure 19. The turbulent kinetic energy increases slightly as the bubbles start to modify the flow, both near the walls as well as in the middle of the channel, but at this time the distribution has not changed in any fundamental way. The dissipation rate shows a similar structure as the streamwise vorticity squared and increases both near the walls and in the middle of the channel.

As the void fraction distribution in figure 14 shows most clearly, the flow is evolving and given the steady state results for smaller systems and lower Reynolds numbers we expect its structure to continue to change. It is, however, noticeable that some aspects, such as the average velocity has not changed much for the time examined here. This suggest that care must be exercised when interpreting short time results for turbulent bubbly flows since the results may appear to be at steady state whereas they actually are evolving on a relatively long timescale. Furthermore, the results suggest that it is important to follow the evolution for a longer time to capture fully the modification that the bubbles have on the flow.

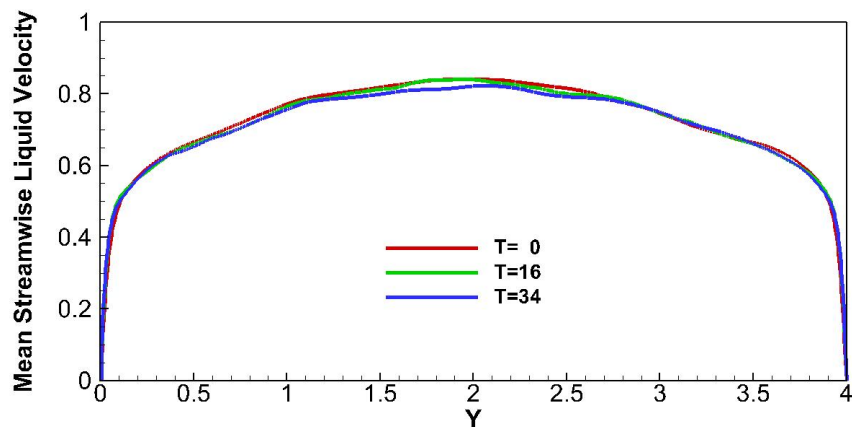


Figure 12. The mean streamwise liquid velocity across the channel at different times.

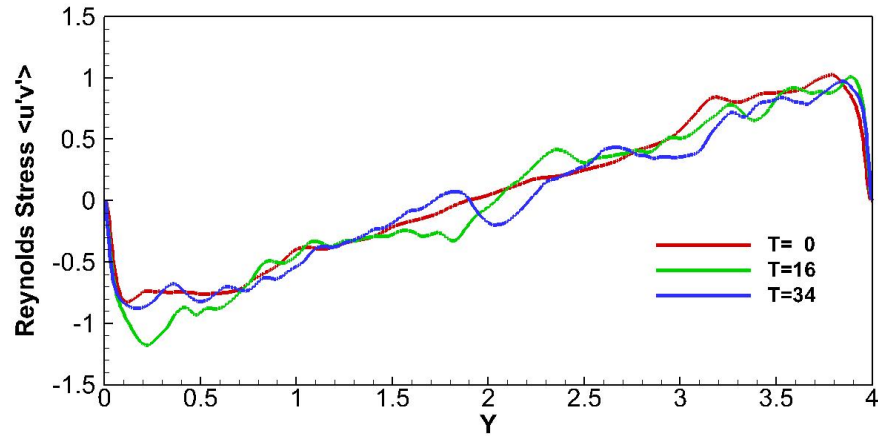


Figure 13. The Reynolds stresses (normalized by $(u^+)^2$, where u^+ is the friction velocity) across the channel at different time steps.

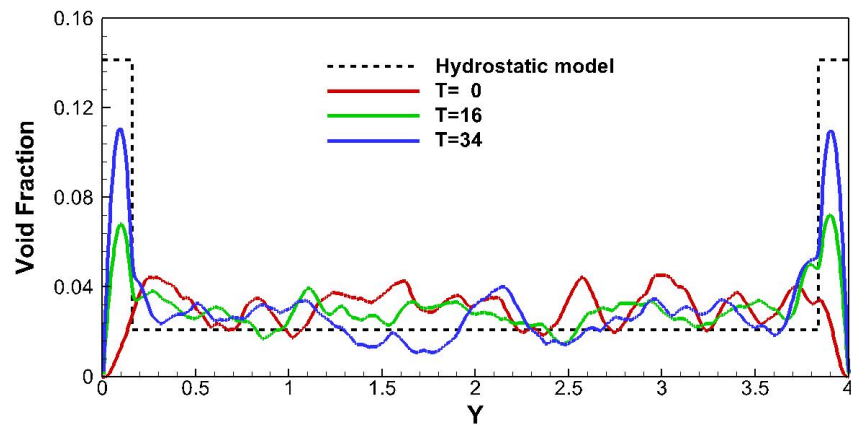


Figure 14. The void fraction at three different times, along with the predictions of a simple model for the void fraction at steady state.

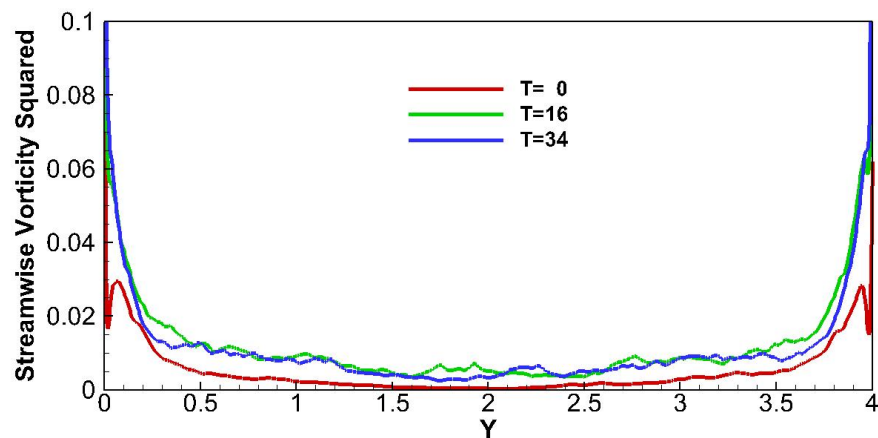


Figure 15. The streamwise vorticity squared (normalized by $1/t_0^2$, where t_0 is a reference time equal to μ/τ_w) across the channel at different time steps.

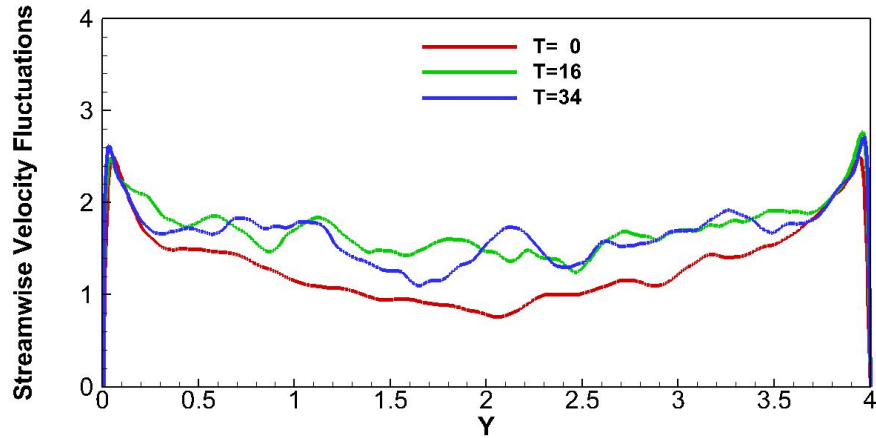


Figure 16. The streamwise velocity fluctuations (normalized by u^+ , where u^+ is the friction velocity) across the channel at different time steps.

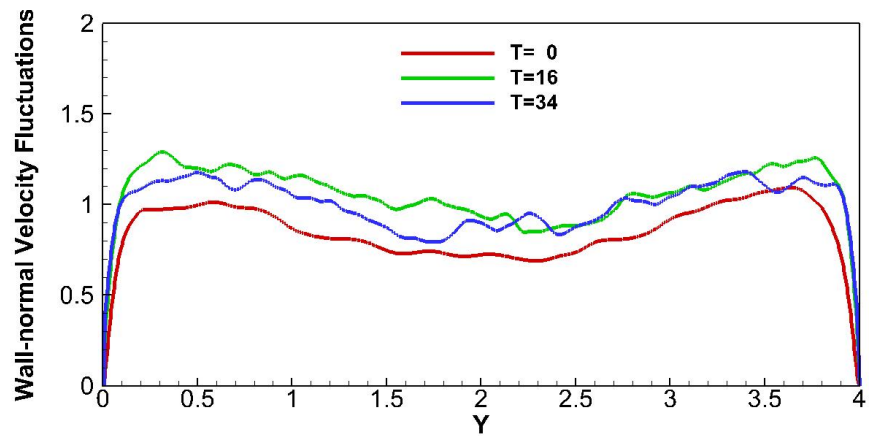


Figure 17. The wall-normal velocity fluctuations (normalized by u^+ , where u^+ is the friction velocity) across the channel at different time step.

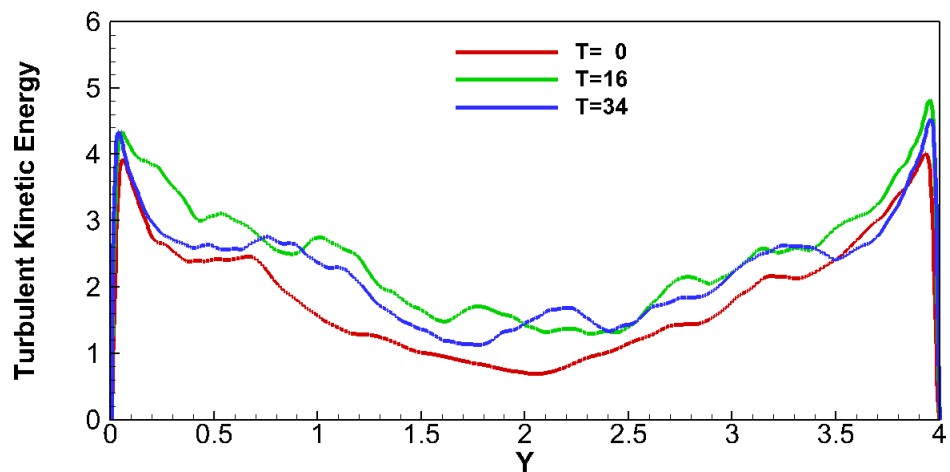


Figure 18. Turbulent Kinetic Energy (normalized by $(u^+)^2$) across the channel.

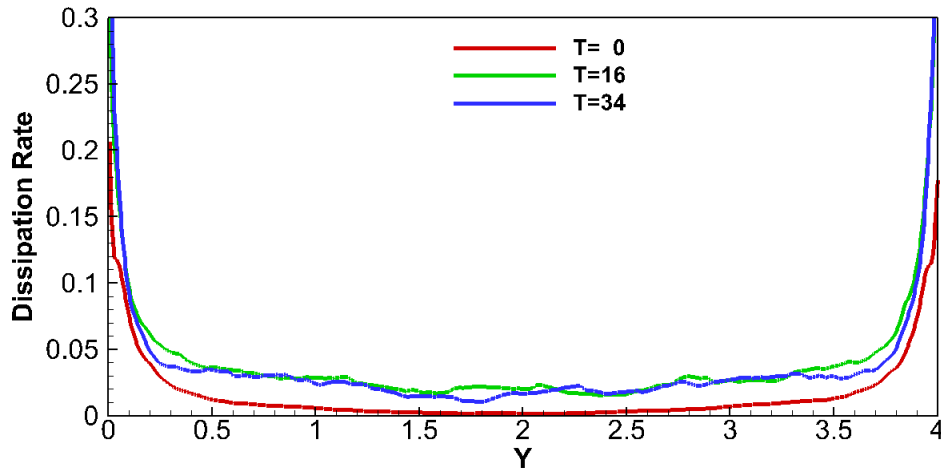


Figure 19. Dissipation Rate (normalized by $(u^+)^4/\nu$) across the channel.

4. Future Work

The results shown here, and our earlier results for the lift and drag on single bubbles have lead to significant new data and insight into bubbly flows. There are, however several aspects that need to be examined further. We expect to address three issues in a follow-on study:

- The importance of turbulent dispersion will be examined by placing bubbles of different sizes near the wall in turbulent channel flow and quantify how fast they move away from the wall. The focus will be on isolated bubbles to reduce the bubble induced turbulent modification and in most of the runs gravity forcing will be taken to be zero to isolate the effect of dispersion.
- Simulations of large bubble systems, with as large range of scales as computationally feasible, focusing on turbulent upflow in a rectangular channel, with a large number of bubbles of different sizes. The focus is on the transient evolution (since the steady state sometimes results in relatively simple flows structures), where the overall structure of the flow, such as void fraction and turbulence intensity are changing. The friction Reynolds number will be 500 or larger, and at least 500 bubbles will be included.
- Exploration of the data to extract information for modeling. Data obtained by averaging over the homogeneous directions and well as local filtering will be collected and we will explore the relations between unknown closure terms and quantities that are evolved in large-eddy and two-fluid simulations, using nonlinear data reduction techniques (such as principal component analysis or more advanced variants).

Given that significant effort was put into the development of additional tools used for the presented studies, it makes good sense to continue the work by expanding the parametric space. The authors will value the feedback from the modeling community with regards to specific gaps which exist in the available experimental database where the DNS/ITM approach can help.

Appendix

FTC3D is a specialized code for direct numerical simulations of multiphase flows. The “one-fluid” Navier-Stokes equations for incompressible flows, where a single set of equations is used for the whole flow domain, are solved on a regular structured staggered grid using an explicit projection method. Time integration is done by a second order predictor-corrector method, the viscous terms are discretized by second-order centered differences and the advection terms are approximated using a QUICK scheme. The pressure equation is solved using a multigrid method or a Krylov scheme (BIGSTAB).

The interface between the different fluids is tracked by connected marker points that are advected with the flow. The interface, or the “front,” consists of points and triangular elements that connect the points. Once the marker points have been advected, a marker function is constructed from the new interface location. The front is also used to compute surface tension, which is then smoothed onto the fluid grid and added to the discrete Navier-Stokes equations. In addition to the computation of the surface tension and the construction of the marker function, the chief challenge in front-tracking is the dynamic updating of the front, whereby marker points are added or deleted to maintain the point density needed to fully resolve the interface. This is done fully automatically as part of the front advection.

The method was introduced by Unverdi & Tryggvason (1992) and for description of the original method, as well as various improvements and refinements, see Tryggvason et al. (2001) and Tryggvason et al. (2011). The method has been used to simulate a large range of multiphase flows, including bubbly flows. See, Bunner & Tryggvason (2002a,b), Esmaeeli & Tryggvason (2005), and Biswas, Esmaeeli & Tryggvason (2005), for example. For other implementation of similar ideas and applications to bubbly flows, see Dijkhuizen et al. (2010a,b); van Sint Annaland et al. (2006); Hao & Prosperetti (2004); Hua & Lou (2007); Muradoglu & Kayaalp (2006), for example.

References for Appendix:

Biswas, S., Esmaeeli, A. & Tryggvason, G. 2005 Comparison of results from DNS of bubbly flows with a two-fluid model for two-dimensional laminar flows. *Int. J. Multiphase Flows* 31, 1036–1048.

Bunner, B. & Tryggvason, G. 2002a Dynamics of homogeneous bubbly flows. Part 1. Rise velocity and microstructure of the bubbles. *J. Fluid Mech.* 466, 17–52.

Bunner, B. & Tryggvason, G. 2002b Dynamics of homogeneous bubbly flows. Part 2. Velocity fluctuations. *J. Fluid Mech.* 466, 53–84.

Bunner, B. & Tryggvason, G. 2003 Effect of bubble deformation on the stability and properties of bubbly flows. *J. Fluid Mech.* 495, 77–118.

Esmaeeli, A. & Tryggvason, G. 2005 A direct numerical simulation study of the buoyant rise of bubbles at $O(100)$ Reynolds number. *Phys. Fluids* 17, 093303.

- Dijkhuizen, W., Roghair, I., Annaland, M. Van Sint & Kuipers, J. 2010a DNS of gas bubbles behaviour using an improved 3d front tracking model—drag force on isolated bubbles and comparison with experiments. *Chem. Eng. Sci.* 65, 1415–1426.
- Dijkhuizen, W., Roghair, I., Annaland, M. Van Sint & Kuipers, J. 2010b DNS of gas bubbles behaviour using an improved 3d front tracking model—model development. *Chem. Eng. Sci.* 65, 1427–1437.
- Hao, Y. & Prosperetti, A. 2004 A numerical method for three-dimensional gas–liquid flow computations. *J. Comput. Phys.* 196, 126–144.
- Hua, J. & Lou, J. 2007 Numerical simulation of bubble rising in viscous liquid. *J. Comput. Phys.* 222, 769–795.
- Muradoglu, M. & Kayaalp, A. D. 2006 An auxiliary grid method for computations of multiphase flows in complex geometries. *J. Comput. Phys.* 214, 858–877.
- Tryggvason, G., Bunner, B., Esmaeeli, A., Juric, D., Al-Rawahi, N., Tauber, W., Han, J., Nas, S. & Jan, Y.-J. 2001 A front tracking method for the computations of multiphase flow. *J. Comput. Phys.* 169, 708–759.
- Tryggvason, G., Scardovelli, R. & Zaleski 2011 *Direct Numerical Simulations of Gas- Liquid Multiphase Flow*. Cambridge University Press.
- Unverdi, S. O. & Tryggvason, G. 1992 A front-tracking method for viscous, incompressible, multi-fluid flows. *J. Comput. Phys.* 100, 25–37.
- van Sint Annaland, M., Dijkhuizen, W., Deen, N.G. & Kuipers, J.A.M. 2006 Numerical simulation of gas bubbles behaviour using a 3D front tracking method. *AIChE J.* 52, 99–110.